

Solution space reduction in the peripheral nerve source localization problem using forward field similarities

José Zariffa^{1,2,3} and Milos R Popovic^{1,2,3,4}

¹ Institute of Biomaterials and Biomedical Engineering, University of Toronto, 164 College Street, Suite 407, Toronto, Ontario M5S 3G9, Canada

² Edward S. Rogers Sr. Department of Electrical and Computer Engineering, University of Toronto, Toronto, Ontario, Canada

³ Rehabilitation Engineering Laboratory, Toronto Rehabilitation Institute, Toronto, Ontario, Canada

E-mail: milos.popovic@utoronto.ca

Received 4 December 2007

Accepted for publication 14 April 2008

Published 6 May 2008

Online at stacks.iop.org/JNE/5/191

Abstract

Improving our ability to localize bioelectric sources within a peripheral nerve would help us to monitor the control signals flowing to and from any limb or organ. This technology would provide a useful neuroscience tool, and could perhaps be incorporated into a neuroprosthesis interface. We propose to use measurements from a multi-contact nerve cuff to solve an inverse problem of bioelectric source localization within the peripheral nerve. Before the inverse problem can be addressed, the forward problem is solved using finite element modeling. A fine mesh improves the accuracy of the forward problem solution, but increases the number of variables to be solved for in the inverse problem. To alleviate this problem, variables corresponding to mesh elements that are not distinguishable by the measurement setup are grouped together, thus reducing the dimension of the inverse problem without impacting on the forward problem accuracy. A quantitative criterion for element distinguishability is derived using the columns of the leadfield matrix and information about the uncertainty in the measurements. Our results indicate that the number of variables in the inverse problem can be reduced by more than half using the proposed method, without having a detrimental impact on the quality of the localization.

(Some figures in this article are in colour only in the electronic version)

1. Introduction

Improvements in our ability to localize bioelectric activity within a peripheral nerve would be useful in several respects. Primarily, such technology would make it easier to characterize the control signals being exchanged between the central nervous system and a limb or organ, thereby allowing us to further our understanding of physiological control systems such as reaching [1] and bladder control [2]. Furthermore, if the localization could be performed in real time, the information flowing to a given limb could be extracted, interpreted and used to control a neural prosthesis.

Unfortunately, existing solutions to this problem have significant shortcomings. Extraneural recordings obtained using nerve cuff electrodes can detect variations in the activity of the nerve as a whole, but techniques to determine the specific location of that activity within the nerve are currently limited. In particular, although the selectivity that can be achieved with cuff electrodes has been studied [3, 4], little work has been done on how to actually identify a combination of active pathways within the nerve using recordings from its surface. Intraneural microelectrode arrays, on the other hand, can give us information about activity close to the tips of the microelectrodes, but arrays dense enough to achieve a good coverage of the nerve are more invasive than cuff electrodes,

⁴ Webpage: www.toronto-fes.ca

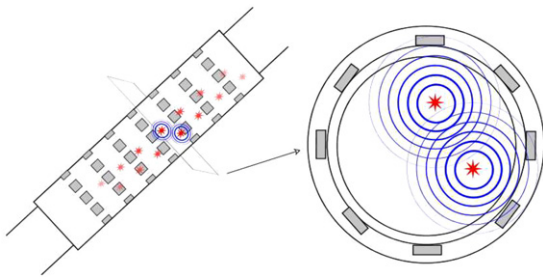


Figure 1. Schematic representation of a multi-contact cuff electrode being used to record the electric potentials generated by the activity within a peripheral nerve. These measurements are then used to solve an inverse problem of source localization.

may inadvertently cause damage to the nerve when implanted or during movement and may be too big for smaller nerves [5].

With this problem in mind, the overall objective of our research is to achieve more precise localization of electrical activity within a nerve than what is possible with existing methods, by approaching the issue as an inverse problem of source localization. Using potential recordings from multiple sites at the periphery of the nerve, obtained from a cuff electrode with a large number of contacts, the problem can be formulated as a modified version of the distributed linear approach to the electroencephalography/magnetoencephalography (EEG/MEG) source localization problem [6–12]. A schematic representation of the proposed measurement setup is shown in figure 1. Although this method uses extraneural recordings, it is differentiated from most of the other methods in this category by the number of electrode contacts and the fact that source localization algorithms are used rather than traditional signal processing techniques. Related approaches that have previously been proposed include the use of blind source separation [13, 14] and linear regression [15] to differentiate the signals in two fascicles. The method we are proposing constitutes a more flexible framework that can be applied both to differentiation between several fascicles and to localization within one fascicle (albeit with limited resolution). A similar source localization approach has been suggested for the purposes of electrode targeting in the spinal cord [16].

The aim of the current study is to reduce the number of variables to be estimated in the source localization problem by taking into account the inherent limitations in the measurement setup. The guiding principle for the reduction will be that if the properties of the nerve, the electrode and the discretization of the solution space are such that the sources at two adjacent locations will produce indistinguishable measurements, then the activity at those two locations can be represented by a single variable. The main benefit of eliminating unnecessary variables will be improvements in computation time and storage requirements, as well as improved insight into what resolution limitations are intrinsic to a given nerve anatomy and electrode geometry.

In source localization problems, including EEG/MEG and the peripheral nerve problem under consideration here, the

relationship between the measurements and electrical activity can be formulated as

$$\mathbf{d} = \mathbf{L}\mathbf{j} + \epsilon, \quad (1)$$

where \mathbf{d} is a vector of N potential measurements obtained from the electrode contacts, \mathbf{j} is a vector of dimension $3M$ containing the magnitudes of dipolar current sources spread throughout the region under consideration (using three orthogonal dipoles at each of the M positions), \mathbf{L} is an $N \times 3M$ matrix describing the influence on each electrode contact of a unit dipole source at each location and orientation in the discretized space and ϵ is the additive noise. \mathbf{L} is known as the leadfield matrix. It is built using a model of the peripheral nerve, with which numerical techniques are used to compute the potentials at every electrode contact for each possible unit source. For EEG/MEG problems, boundary-element methods are generally employed, but the anisotropic nature of the peripheral nerve tissues make finite-element (FE) models more appropriate [17, 18]. The magnitude of each of the three orthogonal dipoles at each of the elements in the FE model is then treated as one variable in the inverse problem of source localization. As a result, M is typically considerably larger than N . Because the inverse problem of recovering the source activations from the measurements is ill-posed, a large number of techniques have been proposed to choose acceptable solutions using various constraints, either anatomical or mathematical in nature (reviews on the topic include [19–22]).

The accuracy of the FE model both in terms of anatomy and tissue conductivities will influence the quality of the solution when the leadfield computed from the model is applied to measurements obtained *in vivo*. When a FE model is used to construct the leadfield, the fineness of the mesh will have a significant impact on the accuracy of the matrix entries. Unfortunately, each element in the mesh corresponds to a variable to be solved for in the inverse problem, creating a conflict between the needs to make the leadfield as accurate as possible and to keep the number of variables as small as possible. A simple way to reduce the number of variables without coarsening the original FE mesh would be to decimate the solution space for the purposes of the inverse problem. Here, we propose an alternative method to reduce the number of variables, where the decisions are based on quantitative information contained in the leadfield. Each column of the leadfield matrix describes the set of measurements obtained when a unit source is placed at a given location (the forward field of that source). Therefore, if the difference between two columns corresponding to adjacent locations is extremely small, then the two corresponding sources can be said to be indistinguishable by the measurement setup. This implies that two variables are being used when only one is useful. We investigate how much reduction in the number of variables can be achieved by grouping together leadfield columns that are indistinguishable, and what, if any, detrimental impact this transformation may have on the process of solving the inverse problem.

The notion of varying the mesh coarseness in accordance with the capabilities of the measurement setup has been

previously proposed in the context of a different inverse problem, electrical impedance tomography (EIT) [23, 24]. By using the differences between leadfield columns as a quantitative grouping criterion, we are adapting this idea to a bioelectric source localization problem, and developing a method by which the accuracy of the forward problem does not need to be compromised. Part of this work has been previously presented at a conference [25].

2. Theory

Determining whether two leadfield columns correspond to indistinguishable elements is equivalent to determining whether all the entries in the two vectors are indistinguishable down to a given precision. The precision of the sensor and the amount of noise present will determine the minimum difference that must exist between two values for them to be reliably distinguishable. Calling this minimum distance δ , the two vectors v_1 and v_2 are deemed distinguishable if they meet the following condition:

$$\|v_1 - v_2\|_\infty > \delta. \quad (2)$$

The remaining necessary step before being able to apply this criterion is to determine δ . We can consider sensor precision and measurement noise within a single framework by interpreting the sensor error as noise. To relate δ to the noise level, two values will be considered distinguishable if they are separated by at least twice the standard deviation of the noise. By using the definition of the noise-to-signal ratio (NSR) in equation (3) (the standard deviation of the elements of the noise vector over the standard deviation of the elements of the signal vector), the condition stated above can be reformulated as shown in equation (4):

$$\text{NSR} = \frac{\text{std}(\text{noise})}{\text{std}(\text{signal})}, \quad (3)$$

$$\|v_1 - v_2\|_\infty > 2 \times \text{NSR} \times \text{std}(\text{signal}). \quad (4)$$

Using this criterion, groups of indistinguishable adjacent elements can be formed. The leadfield columns corresponding to all the elements in a group are then replaced by a single vector equal to the average of all the selected original columns, thereby reducing the total number of columns in the leadfield.

It is typical for the leadfield in a bioelectric source localization problem to contain three columns for each location to be solved for, corresponding to the three orthogonal components of the dipole at that location. In that case, two elements can truly be said to be indistinguishable only if all the three pairs of leadfield columns prove indistinguishable. In addition, in order to guarantee that the elements are indistinguishable for a unit source of any orientation, the threshold in equation (4) must be divided by $\sqrt{3}$. A short proof of this is provided in the appendix. On the other hand, in peripheral nerves, the current sources generating the electric potentials outside of the axon can be modeled as dipoles oriented along the axis of the nerve [26]. We will therefore restrict the solution space to dipoles oriented in that direction only, since the components in the other two directions

Table 1. Parameters for the finite element model of the rat sciatic nerve.

Parameter	Values
Nerve length	5 cm
Endoneurium radius	415 μm
Perineurium width	35 μm
Epineurium width	35 μm
Encapsulation tissue layer width	7.5 μm
Saline layer width	7.5 μm
Cuff length	2.3 cm
Cuff width	30 μm
Cuff radius	500 μm
Cuff starting height	1.35 cm
Saline bath length	5 cm
Saline bath radius	0.485 cm
Endoneurium conductivity (radial)	$8.26 \times 10^{-2} \text{ S m}^{-1}$
Endoneurium conductivity (longitudinal)	0.571 S m^{-1}
Perineurium conductivity (all directions)	$2.1 \times 10^{-3} \text{ S m}^{-1}$
Epineurium conductivity (all directions)	$8.26 \times 10^{-2} \text{ S m}^{-1}$
Encapsulation tissue conductivity (all directions)	$6.59 \times 10^{-2} \text{ S m}^{-1}$
Saline conductivity (all directions)	2 S m^{-1}
Cuff conductivity (all directions)	$1 \times 10^{-7} \text{ S m}^{-1}$

should be significantly smaller. This choice reduces the size of the leadfield from $N \times 3M$ to $N \times M$. Furthermore, the grouping of elements is based on the comparison between a single pair of vectors, instead of three pairs, and using the threshold in equation (4) without adjustment. An analogous reduction would be applicable if the element grouping method was used in an EEG/MEG source localization problem with fixed dipole orientations.

It should be noted that the criterion outlined here assumes that there is no significant difference in the noise level at the various electrode contacts. This is a simplification, because potentials originating from sources outside the cuff vary linearly with the longitudinal position along the cuff [27], such that noise levels will be different for contacts located at different points along the cuff. If sufficient information about the noise distribution at the various contacts was available, it could be incorporated into the distinguishability criterion by making the threshold different for each entry in the vector difference.

3. Methods

3.1. The finite element model and leadfield construction

A finite element model of a unifascicular section of the rat sciatic nerve was used for the purposes of this study. The model consisted of a cylindrical nerve surrounded by a cuff electrode. The nerve consisted of a single fascicle and was modeled as three concentric cylinders representing the endoneurium, perineurium and epineurium layers. The nerve and the cuff were separated by an encapsulation tissue layer and a saline layer. The whole structure was placed in a saline bath. The dimensions and conductivities of the various parts of the nerve model are given in table 1 and based on similar models and anatomical studies described in the literature [3–5, 28–32].

From this model, five meshes of varying coarseness were generated. The solution space for the source localization problem was restricted to the endoneurium. The number of mesh elements for the endoneurium region only was 75 600, 38 400, 19 200, 12 000 and 8400 for the five meshes, respectively. The other variable of interest is the number of contacts in the cuff electrode. Four values were considered: 104, 56, 24 and 12. The 56 contacts were chosen from the original 104, the 24 from the 56 and the 12 from the 24, such that each set was a subset of the previous case (specifically, the contact configurations consisted of 13 rings of 8 contacts, 7 rings of 8 contacts, 3 rings of 8 contacts and 3 rings of 4 contacts, with the rings in all cases being positioned symmetrically with respect to the middle of the cuff). The 56-contact electrode was modeled on a recording cuff design by the Laboratory for Biomedical Microtechnology at the University of Freiburg [33], and the other cases are merely extensions or subsets of this pattern of contacts. The electrode dimensions in the model are also taken from this design, which corresponds to the device that will be used in upcoming acute source localization experiments in rats. The 1 mm diameter of this cuff is very close to the approximate diameter of the rat sciatic nerve, hence the tight fit of the cuff in the model. In total, the 5 coarseness levels and 4 electrode patterns resulted in 20 leadfield matrices. The finite element analysis was conducted using the SCIRun computing environment [34], and the rest of the leadfield computations were performed using the Matlab software. The procedure for obtaining the leadfield from the finite element model is described by Weinstein *et al* [17].

3.2. Element grouping algorithm

The algorithm described in the theory section is designed to reduce a leadfield matrix based solely on the entries of that matrix, rather than using information contained in a specific set of measurements. If we want to incorporate information about the noise level into the choice of threshold, however, the standard deviation of the signal must be known (see equation (4)). In order to circumvent the problem, we base the threshold calculations on a collection of sample signals obtained from the leadfield columns themselves. Each column corresponds to the measurements obtained when a unit source is placed at a given location, and therefore can be seen as a simple sample signal. We choose a subset of all these possible sample signals. For each of the column vectors in this set, the standard deviation of the entries of the vector is computed. The average of these standard deviation values is then used as the signal standard deviation in equation (4). The columns included in the subset are those corresponding to the mesh elements lying in the endoneurium between the heights of 2 and 3 cm along the 5 cm nerve model, under the assumption that the signals originating close to the midpoint of the cuff are the most representative of the signals that we are interested in localizing.

Having now obtained all the information necessary for determining whether two elements are distinguishable, we can proceed to use this criterion to form groups of indistinguishable

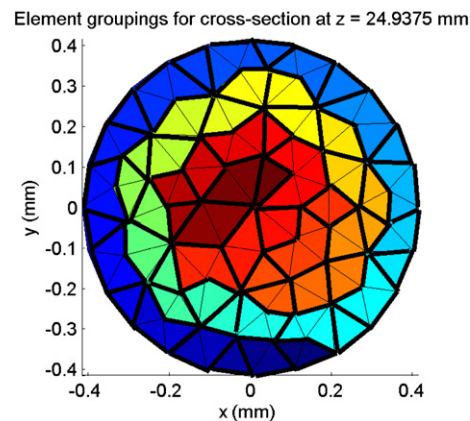


Figure 2. Example of the results obtained when the grouping algorithm is applied to a layer of the FE model at $z = 24.9375$ mm, under the assumption of very low-noise measurements. Elements surrounded by thick lines belong to the same group.

elements. Although, theoretically, groups could consist of non-adjacent elements spread throughout the solution space, the leadfield reduction process could then no longer be interpreted as a search for the inherent resolution achievable by the measurement setup. In this study, the additional restriction is therefore imposed that groups should be formed from connected mesh elements. This has the additional advantage of considerably reducing the time required to test every eligible pair of elements for distinguishability. To further simplify the grouping process, we use the fact that the mesh was constructed using an extrusion process that results in distinct layers of elements, and only compare elements to others within the same layer. Within each layer of the mesh, the algorithm used is as follows. First, a chain of connected elements is formed, going along the outer edge of the layer and spiraling inwards until the center is reached. If a point is reached where all the elements connected to the current element are already part of the chain, then the chain continues at the next free element. Once all the elements have been added, comparisons are performed on successive elements of the chain. For instance, the second and first elements are compared, and if they are indistinguishable they are grouped together. If the third element is also indistinguishable from both of the first elements, it is added to the group. This process is continued until an element is found that cannot be added to the group. A new group is then begun, and so on until all the end of the chain is reached. A sample grouping is shown in figure 2, corresponding to a layer of the FE model midway up the cuff electrode (this particular grouping is based on the assumption of a 0.1% NSR).

The algorithm just described clearly does not capture all possible groupings. The chaining process essentially restricts the comparisons to a one-dimensional geometry instead of a two-dimensional one, and some elements that are indistinguishable will therefore not be grouped. Additionally, restricting the comparisons to elements within the same layer will also omit some possible groupings. The spiral shape is dependent on the geometry of the mesh, which is irregular and so can cause some distortion and influence which elements

are grouped (this effect is visible in figure 2 toward the center of the cross-section). Unfortunately, developing an algorithm able to maximize the number of three-dimensional groupings is far from a trivial task, and is not the main concern of this study. The chain algorithm used is capable of significantly reducing the size of a leadfield, as will be shown in the results section, and therefore is deemed sufficient for the purposes of this study.

The following NSR values were used to choose a grouping criterion: 0.1%, 5%, 10%, 15% and 20%. Having an error equal to 0% is unrealistic, if only because of numerical precision issues. For the purpose of this study, a value of 0.1% was therefore used instead of 0% to capture very small errors, such that elements that are extremely similar will still be grouped together.

3.3. Leadfield comparison metrics

The success of the leadfield reduction process will be evaluated primarily in terms of the number of columns of the reduced leadfield, compared to the original leadfield. Nonetheless, the advantages derived from a smaller matrix may not be worthwhile if the new matrix has a detrimental impact on the quality of the inverse problem solution. For this reason, it is important to have a set of metrics that reflect the difficulty of solving the ill-posed problem using a given matrix.

3.3.1. Rank and condition number. The rank of the leadfield matrix should be equal to the number of electrode contacts. Otherwise, some of the measurements would be linearly dependent on others and not providing any additional information. It is therefore important to check that a reduced leadfield still has full row rank, in order to confirm that the reduction process has not led to a loss of information. The other matrix property that will be examined is the condition number, which is a measure of the sensitivity of the solution of a linear system of equations to errors in the right hand side [35, 36]. The condition number can be computed as the ratio of the largest and smallest singular values of the matrix. Matrices with relatively small condition numbers are said to be well conditioned, otherwise they are ill conditioned. The leadfield matrix in the source localization problem is typically ill conditioned, and a variety of regularization techniques exist to deal with this problem (usually by finding ways to minimize the destabilizing effect of very small singular values, for example by adding a constant to all singular values or by truncating the smallest ones) [36]. Our concern here is therefore not the absolute value of the condition number, but we need to check that the condition number of the reduced leadfield is not significantly greater than that of the original leadfield. Otherwise, the reduction process may have made the problem more difficult to solve. The metric used is therefore the ratio of the condition number of the reduced matrix to that of the original matrix.

3.3.2. Geometry noise. The two main sources of error in the source localization problem are measurement noise and geometry noise. The geometry noise is the error introduced by

inaccuracies in the leadfield matrix, which occur because the models used to solve the forward problem are not completely accurate representations of the true anatomy. During the leadfield reduction process, the columns corresponding to elements deemed indistinguishable are averaged together. Depending on how rigorous a threshold is used, this averaging process could introduce some additional geometry noise. For each column in the original leadfield, a geometry noise vector is defined as the difference between the original leadfield column and the corresponding column in the reduced leadfield. By analogy with the measurement noise, the geometry noise level is then defined by using this geometry noise vector and the original leadfield column in equation (3). The average of this value for all the columns in the original leadfield is then used as a metric quantifying the amount of additional geometry noise introduced by the reduction process. Defining Met1 to be this metric, $signal_i$ to be the i th column of the original leadfield and ge_i to be the geometry error vector corresponding to that column, the metric is computed as shown in the following equation (where M is once again the number of leadfield columns):

$$Met1 = \left(\sum_{i=1}^M \frac{\text{std}(ge_i)}{\text{std}(signal_i)} \right) / M. \quad (5)$$

3.4. Example and complexity analysis

Although the rank, condition number and geometry noise metrics have the advantage of not being dependent on a specific source configuration, it is nonetheless beneficial to consider specific examples. These examples can provide some confirmation that the leadfield reduction process does not significantly increase the localization error, as well as illustrate the reductions in computation time that can be achieved. We focus here on two cases: the 56-contact, 75 600-element model, with 0.1% noise and 10% noise. The reduced leadfields constructed for NSR = 0.1% and NSR = 10% are used for the first and second of those cases, respectively, and the localizations are compared with those obtained using the original leadfield.

For each case, we generate simulated measurements corresponding to an action potential traveling along a single myelinated fiber. A myelinated mammalian nerve fiber action potential is first simulated using the model described by Sweeney *et al* [37]. In order to remain consistent with the EEG/MEG source localization literature, equivalent current dipoles are used to approximate the electrical activity of the nerve fibers. The magnitude waveform of the current dipole is therefore obtained from the first derivative of the transmembrane potential during the action potential [38]. The waveform is then propagated from one node of Ranvier to the next at a speed of approximately 57 m s^{-1} [37]. The nodes of Ranvier are placed 1 mm apart, which is consistent with a $10 \text{ }\mu\text{m}$ -diameter fiber. For the purposes of this example we restrict the localization to a single time instant, when the action potential's peak is in the nodes of Ranvier near the middle of the cuff. Once the current dipole locations and magnitudes have been obtained in this way, the measurements

are computed using the original leadfield and the appropriate amount of noise is added.

The source localization is performed using the sLORETA algorithm [9]. For each of the two example cases, 100 trials are conducted, with the position of the active fiber in the nerve cross-section generated randomly at every trial. To evaluate the results, the three-dimensional solution is projected onto a two-dimensional cross-section, because our primary interest is to determine which pathway is active. From the two-dimensional projection, localization error is obtained as the distance between the true pathway location and the location of the peak of the estimate. The error is averaged over 100 trials for each of the two example cases. Note that in order to compare the results, the reduced estimate is mapped back to the full solution space by assigning to each variable in the original space the value of the corresponding variable in the reduced space.

The computation time gains that can be achieved using the leadfield reduction depends on the algorithm used to solve the inverse problem. In the case of sLORETA, the first step of the algorithm is to solve a minimum-norm least-squares problem, defined in the following equation:

$$\hat{\mathbf{j}} = \arg \min_j \{ \|\mathbf{L}\mathbf{j} - \mathbf{d}\|^2 + \lambda \|\mathbf{j}\|^2 \}, \quad (6)$$

where $\hat{\mathbf{j}}$ is the source estimate and λ is the regularization parameter that balances the model fitting with the constraints on the solution. This form of regularization is known as Tikhonov regularization [39]; as λ increases, emphasis shifts from ensuring a good fit to the data to ensuring that the solution meets the *a priori* constraints (minimum norm in the case of equation (6)). As the amount of noise in the measurements increases, larger values of λ become necessary in order to stabilize the solution and avoid over-fitting due to noise. Here, the value of λ is chosen using the cross-validation functional [40]. The solution to the problem in equation (6) is given in the following equation [12]:

$$\hat{\mathbf{j}} = \mathbf{T}\mathbf{d} = \mathbf{L}^T[\mathbf{L}\mathbf{L}^T + \lambda\mathbf{I}]^{-1}\mathbf{d}. \quad (7)$$

The second step is to normalize the resulting solution using the resolution matrix. The resolution matrix is defined in this case as $\mathbf{R} = \mathbf{T}\mathbf{L}$ and defines the mapping between the actual and estimated source activities (equation (8)):

$$\hat{\mathbf{j}} = \mathbf{T}\mathbf{d} = \mathbf{T}\mathbf{L}\mathbf{j} = \mathbf{R}\mathbf{j}. \quad (8)$$

For perfect localization to be achieved, \mathbf{R} should be the identity matrix, but in practice this can never be the case because the problem is ill-posed. On the other hand, the diagonal of the resolution matrix does provide information on the bias of the solution for each point in the solution space. In sLORETA, the solution from equation (7) is normalized by elements of \mathbf{R} in order to remove this bias, as shown in the following equation:

$$\hat{\mathbf{j}}_l^T (\mathbf{R}_{ll})^{-1} \hat{\mathbf{j}}_l. \quad (9)$$

In the case of constrained orientations, where there is a single variable per dipole location, $\hat{\mathbf{j}}_l$ is simply the magnitude of the l th dipole and \mathbf{R}_{ll} is the l th diagonal entry of the resolution matrix.

Recall that \mathbf{L} is of size $N \times M$, with M much bigger than N . As a result, the examination of equation (7) reveals it to be of complexity $O(MN^2)$. Each diagonal entry of \mathbf{R} can be computed in $O(N)$, such that the total normalization process can be performed in $O(NM)$. The choice of regularization parameter relies on an eigenvalue decomposition that is limited by the rank N of the leadfield [40], and therefore independent of M . We expect to see these complexities reflected in the computational times of the examples when the original and reduced values of M are used.

4. Results

4.1. Size of the reduced leadfield

The number of columns in the original and reduced leadfields are compared in figure 3, for the five meshes, four electrode contact sets and five NSR values. In all cases, the original leadfield could be reduced to half its original size or less. As more measurement uncertainty was incorporated into the choice of threshold, the size of the reduced leadfield decreased. This result is in accordance with expectations, since it implies that noise deteriorates the achievable resolution.

When the grouping threshold were based on the assumption of very low-noise measurements (NSR = 0.1% in figure 3), the number of electrode contacts had very little influence on the number of columns in the reduced leadfield, suggesting that in ideal conditions the geometries and conductivities of the nerve and cuff may be the key factors influencing the reduction achievable, rather than the number of electrode contacts used. On the other hand, when measurement uncertainty was incorporated into the choice of threshold, the number of electrode contacts started to be more important. Figure 3 shows that in those cases the reduced leadfields had progressively more columns as the number of electrode contacts increased, meaning that the increased number of measurements slightly improved the resolution in the presence of noise. The sizes of the reduced leadfields corresponding to the different contact configurations did not, however, vary linearly with the number of contacts. This suggests that an optimal number of contacts could be found, representing a good trade-off between achieving better resolution and increasing the number of necessary contacts. In the present study, the difference between 12 and 24 contacts was very small, implying that very little is to be gained from using the larger of those two sets. On the other hand, the difference between 24 and 56 contacts was appreciable. The difference between 56 and 104 contacts was also noticeable but somewhat smaller, which suggests that out of the four configurations examined, the 56-contact configuration is the best choice for this problem. As the noise level continued to increase and the size of all the reduced leadfields decreased, however, the size differences due to the number of contacts became less significant (compare, for example, the NSR = 5% and NSR = 20% cases in figure 3). In other words, there was a limit to the amount of uncertainty that the number of contacts could compensate for. Finally, it is important to note that all of these observations are valid for all the five meshes investigated.

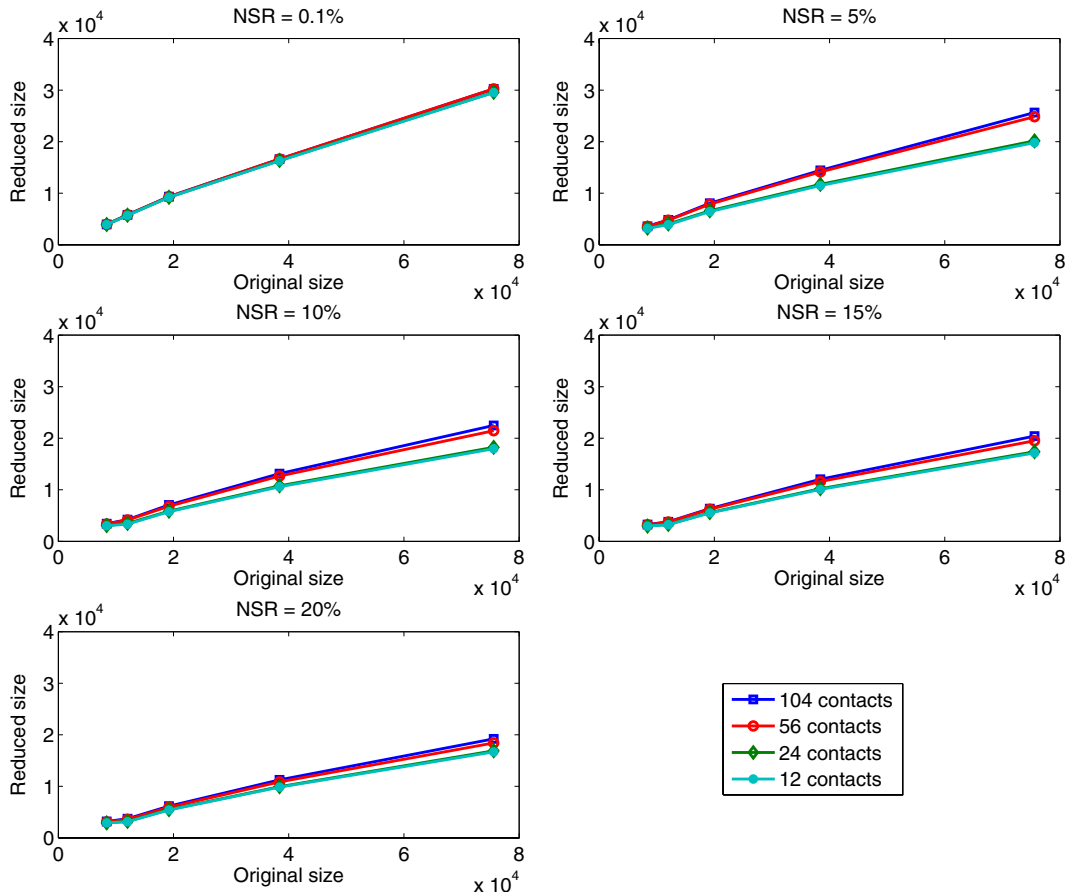


Figure 3. Number of columns of the reduced leadfield as a function of the number of columns of the original leadfield and the number of electrode contacts, when the grouping criterion is based on $NSR = 0.1\%$, 5% , 10% , 15% or 20% . The curves for 104 and 56 electrode contacts nearly overlap, as do the ones for 24 and 12 electrode contacts.

4.2. Properties of reduced leadfield

The reduced matrices had full row rank for every combination of mesh, number of contacts and noise level, meaning that the reduction process never led to any measurements becoming linearly dependent on others.

The ratio of condition numbers between the reduced and original leadfields was in all cases smaller than 1, indicating that none of the leadfields became more ill conditioned than they already were as a result of the reduction process. The mean of these ratios for all the reduced leadfields constructed was 0.905 ± 0.043 , although no significant relationship to the mesh coarseness, number of contacts or noise level was observed.

Table 2 shows the values of the Met1 metric for all of the reduced leadfields. As expected, the amount of geometry error increases as the criterion for indistinguishability is relaxed (a clear example is provided by the row in bold). For all cases, the geometry error remained relatively small, with Met1 remaining under 2.5% when the least stringent grouping criterion is used and under 1% when the most stringent criterion is used. These values suggest that the increased geometry error is a small enough price to pay for the significant reduction that was achieved in the number of variables.

4.3. Simulation results

Figure 4 shows the 2D projections of the results of one trial in the 0.1% noise case, using both the original and reduced leadfields. It is clear from the figure that the localization performance for this trial was virtually identical regardless of whether the original or the reduced leadfield was used. Table 3 displays the average over 100 trials of the localization error for both examples, with the original and reduced leadfields in each case. The results show that the mesh reduction process resulted in a negligible localization error increase in the first example and a small decrease in the second example. These results support our claim that the reduction process does not significantly reduce the quality of the inverse problem solution.

Table 4 displays the total computation times for the two examples, as well as the breakdown into the different components of the algorithm. The table also shows the ratios of these different values for the simulations conducted with the original and reduced leadfields. The computation times were obtained using Matlab (The Mathworks Inc., Natick, MA) running on a desktop PC with a 3.0 GHz Pentium IV processor. As expected, the reduction had no effect on the speed of the regularization process, and the ratio of computation times

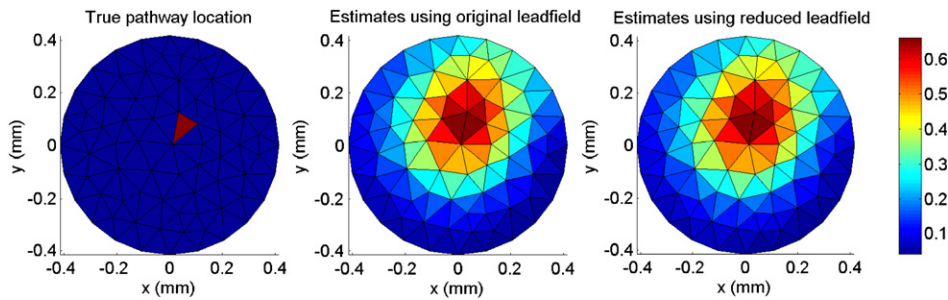


Figure 4. 2D projections of the true source distribution (left), the estimate obtained with the original leadfield (middle) and the estimate obtained with the reduced leadfield (right), for one trial in the NSR = 0.1% example.

Table 2. Metric Met1 for all test cases.

	NSR = 0.1%	NSR = 5%	NSR = 10%	NSR = 15%	NSR = 20%
104 contacts					
75 600 elements	0.6 ± 1.4%	1.1 ± 1.7%	1.3 ± 1.7%	1.6 ± 1.8%	1.8 ± 1.9%
38 400 elements	0.6 ± 1.5%	1.1 ± 1.9%	1.4 ± 1.9%	1.6 ± 1.9%	1.9 ± 2.0%
19 200 elements	0.7 ± 1.8%	1.3 ± 2.3%	1.6 ± 2.3%	2.0 ± 2.3%	2.1 ± 2.3%
12 000 elements	0.7 ± 2.3%	1.3 ± 2.7%	1.7 ± 2.7%	1.9 ± 2.7%	2.0 ± 2.7%
8 400 elements	0.4 ± 1.6%	0.7 ± 2.1%	0.9 ± 2.2%	1.2 ± 2.2%	1.3 ± 2.3%
56 contacts					
75 600 elements	0.6 ± 1.4%	1.1 ± 1.7%	1.4 ± 1.7%	1.7 ± 1.8%	2.0 ± 2.0%
38 400 elements	0.6 ± 1.5%	1.1 ± 1.9%	1.4 ± 1.9%	1.7 ± 2.0%	2.0 ± 2.1%
19 200 elements	0.7 ± 1.8%	1.3 ± 2.3%	1.7 ± 2.3%	2.0 ± 2.3%	2.2 ± 2.4%
12 000 elements	0.7 ± 2.3%	1.4 ± 2.7%	1.7 ± 2.7%	1.9 ± 2.7%	2.1 ± 2.7%
8 400 elements	0.4 ± 1.6%	0.7 ± 2.1%	1.0 ± 2.2%	1.2 ± 2.2%	1.4 ± 2.3%
24 contacts					
75 600 elements	0.6 ± 1.4%	1.3 ± 1.7%	1.6 ± 1.8%	1.9 ± 2.1%	2.1 ± 2.5%
38 400 elements	0.6 ± 1.6%	1.3 ± 1.8%	1.6 ± 1.9%	1.9 ± 2.2%	2.1 ± 2.5%
19 200 elements	0.7 ± 1.8%	1.5 ± 2.2%	2.0 ± 2.3%	2.2 ± 2.5%	2.4 ± 2.7%
12 000 elements	0.8 ± 2.4%	1.6 ± 2.7%	1.9 ± 2.7%	2.1 ± 2.7%	2.2 ± 2.8%
8 400 elements	0.4 ± 1.6%	0.9 ± 2.1%	1.1 ± 2.2%	1.3 ± 2.4%	1.4 ± 2.6%
12 contacts					
75 600 elements	0.6 ± 1.4%	1.3 ± 1.7%	1.7 ± 1.9%	2.0 ± 2.2%	2.2 ± 2.6%
38 400 elements	0.6 ± 1.6%	1.4 ± 1.9%	1.7 ± 2.0%	2.0 ± 2.3%	2.2 ± 2.7%
19 200 elements	0.7 ± 1.8%	1.6 ± 2.2%	2.1 ± 2.4%	2.3 ± 2.6%	2.4 ± 2.7%
12 000 elements	0.8 ± 2.4%	1.7 ± 2.7%	2.0 ± 2.7%	2.1 ± 2.8%	2.3 ± 3.0%
8 400 elements	0.4 ± 1.6%	0.9 ± 2.1%	1.2 ± 2.2%	1.4 ± 2.4%	1.5 ± 2.6%

Table 3. Simulation results using the original and reduced leadfields. All simulations were conducted with 56 contacts, and all means correspond to 100 trials. The size of the original leadfield is 75 600.

	NSR = 0.1%	NSR = 10%
Size of the reduced leadfield	30 252	21 472
Mean localization error using the original leadfield (mm)	0.0801 ± 0.0505	0.1359 ± 0.1108
Mean localization error using the reduced leadfield (mm)	0.0807 ± 0.0505	0.1333 ± 0.0940

for the normalization step was roughly equal to the ratio of the number of variables in the two leadfields. The ratio for the solution of the minimum-norm least-squares problem was slightly larger than expected, but a substantial reduction was nonetheless achieved. The discrepancy between the expected and observed reduction may be due to the fact that our analysis was based on a ‘naive’ approach to matrix multiplications and

did not take into account any of the optimizations that may be present in the Matlab software.

5. Discussion

By using the similarity of leadfield columns as a criterion for grouping several mesh elements into a single variable, we were able to achieve substantial reductions in the number of variables that the inverse problem aims to estimate. This solution space reduction was investigated in the context of the peripheral nerve source localization problem, although it could also be applied to other bioelectric source localization tasks. The reduction is valuable for several reasons. First, the inverse problem is made less ambiguous by the clearer distinctions between the leadfield columns. The smaller discrepancy between the number of measurements and the number of variables also means that the problem will be somewhat better conditioned. Another important consideration is that the smaller leadfield matrix will translate into faster

Table 4. Computation time comparison for simulations using the original and reduced leadfields (all values are means over 100 trials).

Computation step	Computation time (original)	Computation time (reduced)	Ratio (reduced/original)
NSR = 0.1% ($M_{\text{reduced}}/M_{\text{original}} = 0.4$)			
Regularization	0.3136 s	0.3046 s	0.9918
Minimum-norm least-squares	0.3926 s	0.2467 s	0.4865
Normalization	0.3532 s	0.1397 s	0.3959
Total	1.0594 s	0.6910 s	0.6123
NSR = 10% ($M_{\text{reduced}}/M_{\text{original}} = 0.284$)			
Regularization	0.2611 s	0.2615 s	1.0022
Minimum-norm least-squares	0.3290 s	0.1176 s	0.3576
Normalization	0.3427 s	0.0953 s	0.2781
Total	0.9328 s	0.4743 s	0.5087

computations. This can be particularly advantageous when iterative algorithms are used (e.g. FOCUSS [41]), and would become crucial if the real-time implementation were attempted as part of a control system for a neural prosthesis. The reduction in required storage space would also be valuable for implanted systems. The reduction process did not have a negative impact on any of the metrics used to assess the difficulty of the inverse problem.

Despite these advantages, however, it should be kept in mind that the smaller number of variables is a mixed blessing, since it implies lower resolution. The purpose of the technique presented here is not to make the number of variables arbitrarily small, but rather to try to approach the number that best represents the inherent resolution that is achievable for the given nerve properties and measurement setup, without having superfluous variables that simply make the problem more difficult. In that sense, the proposed technique provides us with information that could not be obtained using a simple decimation approach, and is therefore preferable even if both methods provide the same amount of solution space reduction.

The incorporation of information about the noise level in the criterion to determine the distinguishability of two mesh elements was also explored. Not surprisingly, increasing the uncertainty increased the number of element groupings, because pairs that were only barely distinguishable using perfect measurements could no longer be reliably separated. This is simply another way of saying that uncertainty in the measurements will negatively impact the achievable resolution. Additionally, it was found that a large number of electrode contacts had more impact on grouping decisions when uncertainty was present. Indeed, having more contacts would provide better spatial sampling of the electric fields, and therefore provide more opportunities to detect differences between the fields generated by sources in adjacent locations when very small differences are obscured by noise. This finding argues in favor of using a large number of contacts in practice, where noise cannot be completely avoided. On the other hand, it was found that increasing the number of contacts past a certain number started yielding diminishing returns, suggesting that an optimal number could be found. The impact of the number of contacts on the selectivity of cuff electrodes has been previously studied by Yoo and Durand [4], who also noted the existence of a plateau. The optimal number in that study proved to be 7, however there was a single ring

of contacts. The higher number found here suggests that it is possible to take better advantage of having more contacts by distributing them in several rings along the length of the cuff, rather than a single ring. It is important to clarify that our conclusion about the existence of an optimal number of contacts applies only to improvements in resolution, and says nothing about the impact that a larger number of measurements will have on the accuracy of the inverse problem solution. That topic requires further study, but is beyond the scope of this paper.

Note also that, in practice, precise information on the noise level may in many cases be unavailable, in which case grouping decisions will have to be based on the NSR = 0.1% criterion, or on a conservative noise estimate. Otherwise, some resolution might be needlessly lost.

It should be kept in mind when analyzing the results of this study that the specific size reductions achieved are dependent on the grouping algorithm, which is not optimized. Small changes in the algorithm will affect both the groupings that are formed among indistinguishable elements and the overall number of groupings. It would therefore be worthwhile to continue improving the grouping algorithm in order to maximize the achievable reduction. Nonetheless, the present study demonstrated that even with a simple algorithm a substantial decrease in the number of variables could be obtained, highlighting the usefulness of this solution space reduction technique.

Another factor that was fixed in this study was the geometry of the nerve. Although the geometry was simplified here to a single cylindrical fascicle, the solution space reduction technique is in no way dependent on this geometry. It can be applied to any mesh geometry for which a leadfield has been computed. Certain situations, such as a mesh that is not comprised of well-defined layers or whose cross-section is not roughly compatible with a spiral shape, may require modifications of the grouping algorithm, but the basic reduction strategy would remain valid. Changing the geometry would of course alter the exact amount of reduction achieved, but since the technique proposed here is simply exploiting the limited resolution inherent in cuff electrode measurements, substantial reductions should be achievable regardless of the details of the geometry. Likewise, the exact impact of the geometry on the relationship between the number of contacts and the amount of reduction has not yet been established

in the general case, but the underlying insight that having more contacts can compensate up to a point for the loss of information due to noise is independent of geometry.

Finally, although a detailed analysis of the accuracy and resolution that can be achieved using a source localization approach to identify the active pathways in a peripheral nerve is beyond the scope of this paper and will be conducted in upcoming publications, a few general remarks regarding the method are in order. In the EEG/MEG context, source localization techniques have both a much higher temporal resolution and a lower spatial resolution than other modalities, such as fMRI. In the peripheral nerve case, the high temporal resolution remains quite attractive, because of the short time spans involved in trains of action potentials. The low spatial resolution remains an area in obvious need of improvement but, in contrast with the EEG/MEG context, alternative methods for achieving spatial discrimination of the electrical activity within a nerve without risking tissue damage are very limited. EEG/MEG source localization studies are also hindered by the difficulty of assessing the correctness of the results, which is particularly important in light of the ill-posed nature of the problem, but in peripheral nerves the technique would be easier to validate using simultaneous micro-electrode array recordings. The drawbacks of the approach are, first, that a reasonably good model of the nerve anatomy is required in the forward problem to avoid an unacceptably inaccurate leadfield, and second, the sensitivity to noise (although this last point is complex and dependent on the specific algorithm and regularization technique employed). That said, with sufficient anatomical information and careful pre-processing of the nerve cuff signals to minimize the noise, the method could localize sources in a volume conductor of arbitrary complexity. The number of pathways that could be localized simultaneously would be influenced by the resolution of the specific source localization algorithm used (for instance, the sLORETA algorithm used in this paper trades off resolution in favor of accuracy). It is important to note that ‘pathway’ is not equivalent to a single source. In the example presented earlier in this paper, one pathway was modeled using 50 sources placed at consecutive nodes of Ranvier, and was localized accurately.

Based on these considerations, the source localization approach could provide a valuable tool for neural system identification. In addition, being able to simultaneously monitor the action potentials traveling along several specific pathways would have numerous applications in neuroprosthetic systems, in which the activity in a given pathway or pathways could be translated into the detection of specific events (e.g. heel strike) [42, 43] or tracking of movement trajectories [44, 45]. These applications would require the real-time application of the source localization and, although our current software implementation does not quite meet those requirements (see table 4), hardware implementations and computational advances in the next few years make this a realistic target. The solution space reduction method presented in this paper represents a significant advance toward this goal.

Acknowledgments

The authors would like to thank Dr Adrian Nachman for useful discussions. We are also grateful to the Natural Sciences and Engineering Research Council of Canada and the Walter C Sumner Foundation for supporting this work.

Appendix. Threshold adjustment for the case of unconstrained source orientations

In the case of unconstrained source orientations, we want to ensure that two adjacent mesh elements are grouped only if the measurements produced by a unit source in one element are indistinguishable by those produced by the same source placed in the other element, regardless of the orientation of the source. In other words, if there exists a source orientation that results in distinguishable measurements for a unit source, then the two mesh elements should not be grouped. If the elements are distinguishable for one of the three orthogonal orientations corresponding to the leadfield columns, then they are not grouped and no further examination is necessary. Therefore, for the rest of this discussion, the following inequalities are assumed to be true:

$$\|v_{11} - v_{21}\|_{\infty} \leq \delta, \quad (\text{A.1})$$

$$\|v_{12} - v_{22}\|_{\infty} \leq \delta, \quad (\text{A.2})$$

$$\|v_{13} - v_{23}\|_{\infty} \leq \delta, \quad (\text{A.3})$$

where v_{11}, v_{12} and v_{13} are the three leadfield columns corresponding to the first mesh element, and v_{21}, v_{22} and v_{23} are those corresponding to the second mesh element. If the orientation of the source is described by the triplet (a, b, c) , then the measurements produced when that source is placed in the first of the two mesh elements will be given by $av_{11} + bv_{12} + cv_{13}$, with an analogous expression for the second mesh element. The difference between the measurements produced by that source in each of the two mesh elements will then satisfy the following inequality, which follows from equations (A.1) to (A.3) and the properties of the infinity norm:

$$\|a(v_{11} - v_{21}) + b(v_{12} - v_{22}) + c(v_{13} - v_{23})\|_{\infty} \leq (a + b + c)\delta. \quad (\text{A.4})$$

Because the source under consideration has a unit magnitude, the values (a, b, c) must satisfy the constraint

$$\sqrt{a^2 + b^2 + c^2} = 1. \quad (\text{A.5})$$

It is easily verified that the highest value of $(a + b + c)$ attainable under constraint (A.5) is $\sqrt{3}$. Combining this information with equation (A.4), we can conclude that in order to guarantee that the measurement difference will remain under a certain threshold Δ regardless of the orientation of the unit source, then the threshold used in equations (A.1)–(A.3) should be equal to $\delta = \Delta/\sqrt{3}$.

References

- [1] Scott S H 2004 Optimal feedback control and the neural basis of volitional motor control *Nat. Rev. Neurosci.* **5** 532–46
- [2] Rijkhoff N J 2004 Neuroprostheses to treat neurogenic bladder dysfunction: current status and future perspectives *Child Nerv. Syst.* **20** 75–86
- [3] Perez-Orive J and Durand D M 2000 Modeling study of peripheral nerve recording selectivity *IEEE Trans. Rehab. Eng.* **8** 320–9
- [4] Yoo P B and Durand D M 2005 Selective recording of the canine hypoglossal nerve using a multicontact flat interface nerve electrode *IEEE Trans. Biomed. Eng.* **52** 1461–9
- [5] Navarro X, Krueger T B, Lago N, Micera S, Stieglitz T and Dario P 2005 A critical review of interfaces with the peripheral nervous system for the control of neuroprostheses and hybrid bionic systems *J. Peripher. Nerv. Syst.* **10** 229–58
- [6] Hamalainen M S and Ilmoniemi R J 1994 Interpreting magnetic fields of the brain: minimum norm estimates *Med. Biol. Eng. Comput.* **32** 35–42
- [7] Pascual-Marqui R D, Michel C M and Lehmann D 1994 Low resolution electromagnetic tomography: a new method for localizing electrical activity in the brain *Int. J. Psychophysiol.* **18** 49–65
- [8] Uutela K, Hamalainen M and Somersalo E 1999 Visualization of magnetoencephalographic data using minimum current estimates *Neuroimage* **10** 173–80
- [9] Pascual-Marqui R D 2002 Standardized low-resolution brain electromagnetic tomography (sLORETA): technical details *Methods Find. Exp. Clin. Pharmacol.* **24** (Suppl. D) 5–12
- [10] Phillips C, Rugg M D and Friston K J 2002 Anatomically informed basis functions for EEG source localization: combining functional and anatomical constraints *Neuroimage* **16** (3 Pt 1) 678–95
- [11] de Peralta Menendez R G, Murray M M, Michel C M, Martuzzi R and Gonzalez Andino S L 2004 Electrical neuroimaging based on biophysical constraints *Neuroimage* **21** 527–39
- [12] Phillips C, Mattout J, Rugg M D, Maquet P and Friston K J 2005 An empirical Bayesian solution to the source reconstruction problem in EEG *Neuroimage* **24** 997–1011
- [13] Tesfayesus W, Yoo P, Moffitt M and Durand D M 2004 Blind source separation of nerve cuff recordings *Proc. 26th Annual Int. Conf. of the IEEE Engineering in Medicine and Biology Society San Francisco, USA* 95–8
- [14] Tesfayesus W and Durand D M 2006 Blind source separation of neural recordings and control signals *Proc. 28th Annual Int. Conf. of the IEEE Engineering in Medicine and Biology Society* 731–4
- [15] Cheng H S, Ju M S and Lin C C 2005 Estimation of peroneal and tibial afferent activity from a multichannel cuff placed on the sciatic nerve *Muscle Nerve* **32** 589–99
- [16] Moffitt M A and Grill W M 2004 Electrical localization of neural activity in the dorsal horn of the spinal cord: a modeling study *Ann. Biomed. Eng.* **32** 1694–709
- [17] Weinstein D, Zhukov L and Johnson C 2000 Lead-field bases for electroencephalography source imaging *Ann. Biomed. Eng.* **28** 1059–65
- [18] Seger M, Fischer G, Modre R, Messnarz B, Hanser F and Tilg B 2005 Lead field computation for the electrocardiographic inverse problem—finite elements versus boundary elements *Comput. Methods Programs Biomed.* **77** 241–52
- [19] Fuchs M, Wagner M, Kohler T and Wischmann H A 1999 Linear and nonlinear current density reconstructions *J. Clin. Neurophysiol.* **16** 267–95
- [20] Pascual-Marqui R D 1999 Review of methods for solving the EEG inverse problem *Int. J. Bioelectromagnet.* **1** 75–86
- [21] Michel C M, Murray M M, Lantz G, Gonzalez S, Spinelli L and de Peralta Menendez R G 2004 EEG source imaging *Clin. Neurophysiol.* **115** 2195–222
- [22] Darvas F, Pantazis D, Kucukaltun-Yildirim E and Leahy R M 2004 Mapping human brain function with MEG and EEG: methods and validation *Neuroimage* **23** (Suppl. 1) S289–99
- [23] Cheney M, Isaacson D, Newell J C, Simske S and Goble J 1990 NOSER: an algorithm for solving the inverse conductivity problem *Int. J. Imag. Syst. Technol.* **2** 66–75
- [24] Isaacson D 1986 Distinguishability of conductivities by electric current computed tomography *IEEE Trans. Med. Imaging* **5** 91–5
- [25] Zariffa J and Popovic M R 2007 Finite element mesh reduction guidelines for the inverse problem of source localization in peripheral nerves *Proc. 30th CMBE Conf.*
- [26] Malmivuo J and Plonsey R 1995 *Bioelectromagnetism: Principles and Applications of Bioelectric and Biomagnetic Fields* (New York: Oxford University Press)
- [27] Andreassen L N and Struijk J J 2003 Artefact reduction with alternative cuff configurations *IEEE Trans. Biomed. Eng.* **50** 1160–6
- [28] Schmalbruch H 1986 Fiber composition of the rat sciatic nerve *Anat. Rec.* **215** 71–81
- [29] Goodall E V, Kosterman L M, Holsheimer J and Struijk J J 1995 Modeling study of activation and propagation delays during stimulation of peripheral nerve fibers with a tripolar cuff electrode *IEEE Trans. Rehab. Eng.* **3** 272–82
- [30] Meier J H, Rutten W L C and Boom H B K 1998 Extracellular potentials from active myelinated fibers inside insulated and noninsulated peripheral nerve *IEEE Trans. Biomed. Eng.* **45** 1146–54
- [31] Parrini S, Delbeke J, Romero E, Legat V and Veraart C 1999 Hybrid finite elements and spectral method for computation of the electric potential generated by a nerve cuff electrode *Med. Biol. Eng. Comput.* **37** 733–6
- [32] Choi A Q, Cavanaugh J K and Durand D M 2001 Selectivity of multiple-contact nerve cuff electrodes: a simulation analysis *IEEE Trans. Biomed. Eng.* **48** 165–72
- [33] Schuettler M, Triantis I F, Rubehn B and Stieglitz T 2007 Matrix cuff electrodes for fibre and fascicle selective peripheral nerve recording and stimulation *Proc. 12th Annual Conf. IFEES Philadelphia, PA*
- [34] SCIRun: A Scientific Computing Problem Solving Environment. Scientific Computing and Imaging Institute (SCI), <http://software.sci.utah.edu/scirun.html>, 2002
- [35] Golub G H and Van Loan C F 1996 *Matrix Computations* (Baltimore, MD: Johns Hopkins University Press)
- [36] Hansen P C 1998 *Rank-Deficient and Discrete Ill-posed Problems: Numerical Aspects of Linear Inversion* (Philadelphia: SIAM)
- [37] Sweeney J D, Mortimer J T and Durand D 1987 Modeling of mammalian myelinated nerve for functional neuromuscular stimulation *Proc. 9th Annual Int. Conf. of the IEEE Engineering in Medicine and Biology Society* pp 1577–8
- [38] Plonsey R 1977 Action potential sources and their volume conductor fields *Proc. IEEE* **65** 601–11
- [39] Tikhonov A N and Arsenin V Y 1977 *Solutions of Ill-posed Problems* (Washington, DC: Winston)
- [40] Pascual-Marqui R D 1999 Reply to comments made by R. Grave de Peralta Menendez and S.L. Gozalez Andino *Int. J. Bioelectromagnet.* **1**
- [41] Gorodnitsky I F, George J S and Rao B D 1995 Neuromagnetic source imaging with FOCUSS: a recursive weighted minimum norm algorithm *Electroencephalogr. Clin. Neurophysiol.* **95** 231–51

- [42] Hansen M, Haugland M K and Sepulveda F 2003 Feasibility of using peroneal nerve recordings for deriving stimulation timing in a foot drop correction system *Neuromodulation* **6** 68–77
- [43] Hansen M, Haugland M K and Sinkjaer T 2004 Evaluating robustness of gait event detection based on machine learning and natural sensors *IEEE Trans. Neural. Syst. Rehabil. Eng.* **12** 81–8
- [44] Micera S, Jensen W, Sepulveda F, Riso R R and Sinkjaer T 2001 Neuro-fuzzy extraction of angular information from muscle afferents for ankle control during standing in paraplegic subjects: an animal model *IEEE Trans. Biomed. Eng.* **48** 787–94
- [45] Cavallaro E, Micera S, Dario P, Jensen W and Sinkjaer T 2003 On the intersubject generalization ability in extracting kinematic information from afferent nervous signals *IEEE Trans. Biomed. Eng.* **50** 1063–73